Inorganic Chemistry

Article

pubs.acs.org/IC

Solid-State Electrochemistry of a Semiconducting MMX-Type Diplatinum Iodide Chain Complex

Hiroaki Iguchi,*[,†,‡] Ayman Nafady,[§,∥] Shinya Takaishi,[†,‡] Masahiro Yamashita,[†,‡] and Alan M. Bond*[,§]

[†]Department of Chemistry, Graduate School of Science, Tohoku University, 6-3 Aramaki-Aza-Aoba, Sendai 980-8578, Japan

[‡]Core Research for Evolutional Science and Technology (CREST), Japan Science and Technology Agency (JST), 4-1-8 Kawaguchi, Saitama 332-0012, Japan

[§]School of Chemistry, Monash University, Clayton, Victoria 3800, Australia

[∥]Department of Chemistry, College of Science, King Saud University, PO Box 2455, Riyadh 11451, Saudi Arabia

Supporting Information

ABSTRACT: Electron-transfer-facilitated dissolution, ion insertion, and desorption associated with an MMX-type quasi-one-dimensional iodide-bridged dinuclear Pt complex (MMX chain) have been investigated for the first time. $K_2(NC_3N)[Pt_2(pop)_4I]\cdot 4H_2O$ (**1**) ($NC_3N^{2+} = (H_3NC_3H_6NH_3)^{2+}$; pop = $P_2H_2O_5^{2-}$) is a semiconductor with a three-dimensional coordination-bond and hydrogen-bond network included in the chain. The cyclic voltammetry of **1** was studied by using **1**-modified electrodes in contact with acetonitrile solutions containing electrolyte. The chemical reversibility for oxidation of **1** depended on the electrolyte cation size, with large cations such as tetrabutylammonium (Bu_4N^+) being too large to penetrate the pores formed by the loss of K^+ and NC_3N^{2+} upon oxidation. The potential for reduction of **1** decreased as the cation size increased. The presence of the acid induced additional well-defined processes but with gradual solid dissolution, attributed to the breaking of the coordination-bond networks.

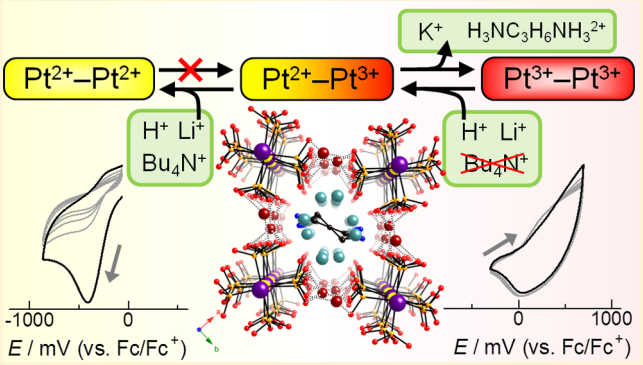

INTRODUCTION

Metal−organic frameworks (MOFs) have been the subject of intense study over the past two decades because of their applications in gas storage[1] and separation,[2] catalysis,[3] and magnetism,[4] as a precursor for gels,[5] and for their ability to act as a host for organic molecules.[6] The electrochemical behavior of MOFs also has been of interest recently[7] from the standpoint of developing rechargeable batteries,[8] supercapacitors,[9] fuel cells,[10] photovoltaics,[11] electrochromic thin films,[12] etc. However, the low conductivity of MOFs limits their performance even if the building blocks used to generate the MOFs have intrinsically good electrochemical properties. Although a few proton-conductive[10] and metal-ion-conductive[13] MOFs have been reported, electron-conductive MOFs are still rare. $[\{Rh_2(acam)_4\}_2I]_n\cdot 6nH_2O$[14] and $Cu[M(pdt)_2]$ (Hacam = acetamide; pdt = 2,3-pyrazinedithiolate) (M = Cu,[15a] Ni[15b]) are representative examples of electron-conductive three-dimensional (3D) MOFs through which the electronic charge carriers can move. Their conductivity can be controlled by the removal or insertion of the guest molecule. Other electron-conductive MOFs described in the literature have conducting $\pi-\pi$ stacked arrays.[16] Since valence fluctuation is a key to achieving high electron conductivity, quasi one-dimensional (1D) halogen-bridged dinuclear metal complexes (MMX chains) are promising alternatives that can display both electron conductivity and porosity.

MMX chains are paddle-wheel-type dinuclear complexes infinitely bridged by halide ions to give an ···M−M−X−M−M−X··· type material. The 1D electron system associated with these complexes consists of the d_{z^2} orbitals of the metal ions (M) and the p_z orbitals of the bridging halide ions (X). Since the oxidation state is M^{2+} or M^{3+} in the mixed-valence state (Robin−Day class II system)[17] or $M^{2.5+}$ in an averaged-valence state (Robin−Day class III system), charge ordering[18] and high conductivity are induced. MMX chains synthesized to date have been categorized by two ligand systems: dithioacetate (dta), $[M_2(RCS_2)_4I]$ (M = Ni, Pt; R = alkyl chain group)[19] and diphosphite (pop), $A_4[Pt_2(pop)_4X]\cdot nH_2O$ (A = alkali metal, alkyl ammonium, etc.; X = Cl, Br, I; pop = $P_2H_2O_5^{2-}$).[20] Although the dta system shows higher conductivity, its chains are densely packed together by van der Waals interactions and no pore exists. In contrast, some pop complexes have a pore (usually filled with the lattice water) present in the framework, which consists of a 3D coordination-bond and hydrogen-bond network between the chains and countercations. Recently, we

Received: December 4, 2013
Published: March 31, 2014

   dx.doi.org/10.1021/ic402980t | *Inorg. Chem.* 2014, 53, 4022−4028

rationally designed this kind of MMX chain structure by introducing binary countercations, $A_2D[Pt_2(pop)_4I]\cdot nH_2O$ (A^+ = K^+ and Rb^+; D^{2+} = aliphatic diammonium ion; n = 2 and 4).[21] Some of these materials exhibited nonlinear conductance[22] and reversible dehydration/rehydration with change in their electrical conductivity and electronic state. However, the electrochemical behavior of these solids has not been studied even in the hydrated state, although the solution-phase electrochemistry of some discrete diplatinum units in the aqueous electrolyte solution has been reported.[23] Analysis of solid-state electrochemical behavior in MMX chains can provide a platform for developing electrochemical devices based on porous semiconducting coordination compounds. Herein, we describe the electrochemistry of surface-attached $K_2(NC_3N)[Pt_2(pop)_4I]\cdot 4H_2O$ (**1**) (NC_3N^{2+} = $(H_3NC_3H_6NH_3)^{2+}$) (Figure 1), whose electrical conductivity is 1.5×10^{-4} S cm^{-1} at room temperature,[21b] to reveal the electrochemical behavior of MMX chains for the first time.

EXPERIMENTAL SECTION

Materials and Chemicals. $K_2(NC_3N)[Pt_2(pop)_4I]\cdot 4H_2O$ (**1**) was synthesized as reported previously.[21b] Since **1** is soluble in water but insoluble in acetonitrile (MeCN), the electrochemistry of the solid adhered to an electrode was studied in this organic solvent containing $LiClO_4$, $NaPF_6$, $NaClO_4$, KPF_6, Bu_4NPF_6, or Bu_4NClO_4 as the supporting electrolyte. The presence of MeCN does not alter the structure of **1**, as shown from powder X-ray diffraction (PXRD) data provided in Figure S1c of the Supporting Information. $HClO_4$ (60% in water) and TFA (trifluoroacetic acid) were used to provide a proton source. Bu_4NPF_6 and Bu_4NClO_4 were purified by recrystallization from ethanol. Other electrolytes and MeCN were used as received from the manufacturer.

Instrumentation. Cyclic voltammetry and bulk electrolysis experiments were carried out at room temperature 20 ± 2 °C using standard three-electrode cell methodologies with BAS 100B or CV-50W workstations. The working electrode was either a 3 mm diameter glassy carbon (GC) electrode (BAS) or an indium tin oxide (ITO) electrode. The working electrode was polished with an alumina slurry and rinsed thoroughly before each experiment. The reference electrode was Ag/Ag^+ (0.01 M $AgNO_3$ with 0.1 M $(Bu_4N)ClO_4$ or 0.1 M $(Bu_4N)PF_6$ in MeCN). The potential of the reference electrode was calibrated by using ferrocene (Fc) as an external standard, and all potentials are reported versus the ferrocene/ferrocenium reference couple (Fc/Fc^+). The counter electrode was a platinum wire. MeCN solutions were purged with nitrogen gas for at least 15 min before each experiment. Field emission scanning electron microscopy (FE-SEM; Hitachi, S-4300) was used to image the microcrystals adhered to the ITO electrode before and after electrochemical experiments. Energy dispersive X-ray (EDX) spectra were measured by using a Genesis 4000 EDAX instrument.

Electrode-Modification Method. Solid **1** was transferred to the surface of the GC electrode by the mechanical attachment method as follows. Several crystals (1 mg) of **1** were placed on a filter paper or a glass plate. After grinding to microcrystalline size, the GC electrode was pressed onto **1** and rubbed so that a small quantity of solid adhered to the electrode surface to form an array of microcrystalline particles.

RESULTS AND DISCUSSION

Voltammetry of 1 over a Wide Potential Range. The electrochemical behavior of **1** was investigated by cyclic voltammetry. Initially, a **1**-modified GC electrode was immersed in MeCN solution containing $LiClO_4$ as the supporting electrolyte, and the potential cycled over the range of +950 to −850 mV (Figure 2a).

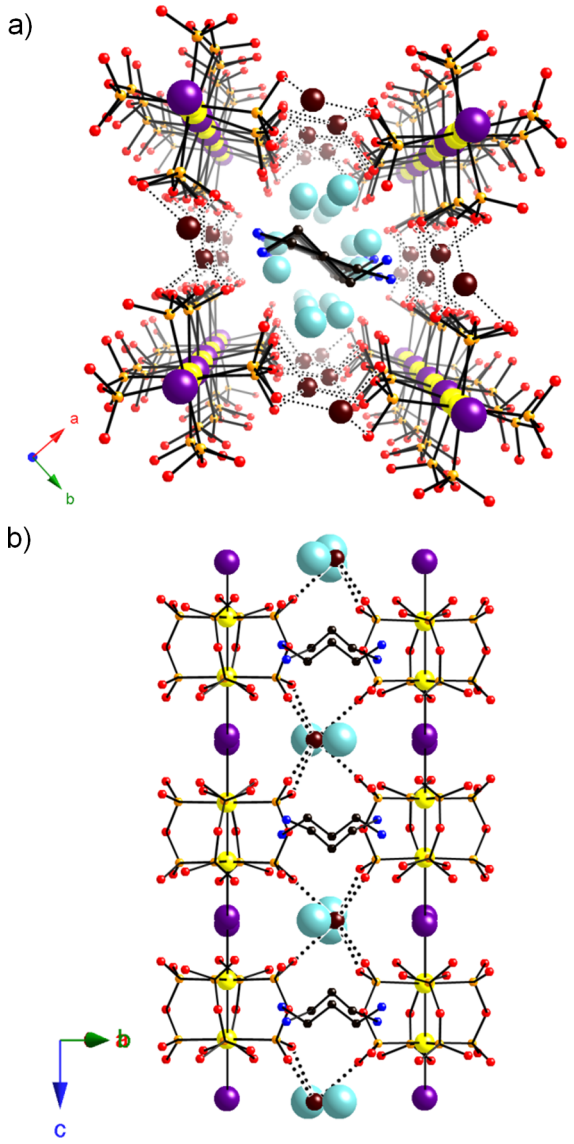

Figure 1. (a) Perspective view along the c-axis and (b) chain structure of **1** (black, C; blue, N; red, O(ligand); light blue, $O(H_2O)$; orange, P; brown, K; purple, I; yellow, Pt). $K^+\cdots O$(ligand) coordination bonds are represented as dotted lines. $K^+\cdots O(H_2O)$ coordination bonds and hydrogen atoms are omitted for clarity. NC_3N^{2+} ions are disordered. Bridging iodide and one of the four crystallographycally independent $O(H_2O)$ are disordered by mirror symmetric operation.

Figure 2a reveals that microcrystals of **1** can be both oxidized and reduced. However, the oxidation and reduction current decreased on cycling the potential, suggesting dissolution of products accompanies electron transfer. The initial oxidation process occurs at about 300 mV, with a companion reduction component at around 0 mV. This process can be assigned to the oxidation of the Pt^{2+}/Pt^{3+} mixed-valent state to the Pt^{3+} state; in the electrochemically induced chemically reversible process, the electron transfer step is not reversible in the sense that the magnitude of the peak separation between the oxidation and reduction components is large and companion reduction potential shifts to more negative values with an increase in scan rate (see Figure S6 and Table S1 in the Supporting Information). The reduction of solid **1** occurs at around −700 mV, which can be assigned as an irreversible reduction from Pt^{2+}/Pt^{3+} mixed-valent state to a Pt^{2+} material.

dx.doi.org/10.1021/ic402980t | Inorg. Chem. 2014, 53, 4022−4028

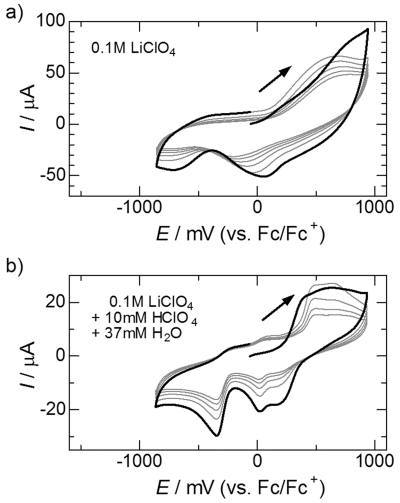

Figure 2. Cyclic voltammograms obtained at a scan rate of 100 mV s^{-1} for oxidation and reduction of a **1**-modified GC electrode in contact with (a) 0.1 M $LiClO_4$ and (b) 0.1 M $LiClO_4$, 10 mM $HClO_4$, 37 mM H_2O in MeCN. First (black) and further (gray) cycles of potential.

Cyclic voltammograms initially scanned to negative potential direction (Figure S3) are similar to those initially scanned in the positive direction (Figure 2), indicating that the redox behavior is essentially independent of the scanning direction when the potential is scanned over the range +950 to −850 mV.

In the case of solutions containing a small amount of $HClO_4$ (with H_2O), all processes become more prominent, as shown in Figure 2b, but additional complexity is found, as the reduction component seen after oxidation splits into two components. The effect of acid will be discussed later. The potential could not be scanned to values more negative than −1000 mV in the presence of acid due to H_2 evolution. The initially colorless solution containing $HClO_4$ gradually changed to yellow (indication of a discrete diplatinum complex) on repetitive cycling of the potential, implying that oxidized and/or reduced products dissolved from solid **1** are soluble in acidified MeCN. However, no color change was detected in neutral conditions. Discussion on the effect of acid and origin of the decrease in the current on cycling the potential will be provided later.

In order to probe the origin of the redox-based chemistry of the mixed-valence diplatinum unit, cyclic voltammograms relevant to the initial oxidation and reduction of surface-confined microcrystals of **1** were studied individually in the presence of different electrolytes.

Effect of Electrolyte Cation on the Oxidation of Solid 1. Cyclic voltammograms in Figure 3 show the electrochemical oxidation of microcrystals of **1** in contact with MeCN solution containing electrolytes with Li^+, Na^+, K^+, or Bu_4N^+ as the cation and either ClO_4^- or PF_6^- as the anion. According to the literature,[24] the combination of electron transfer and insertion of ions from the electrolyte solution into the solid needed to maintain charge neutrality can be achieved by the following mechanisms:

(1) Ions cross the phase boundary and intercalate from the electrolyte into the solid or are lost from the solid without major structural change.[25]
(2) The surface of the solid is fractured and increases in volume, which enables both ions and solvent to penetrate the solid.
(3) Dissolution occurs upon oxidation or reduction.

Since the oxidation process did not depend on the anion, K^+ and/or NC_3N^{2+} ions are probably lost and transferred into the electrolyte upon oxidation. A companion reduction component is evident in Li^+, Na^+, and K^+ solution electrolytes with a peak potential between +50 and −100 mV (Figure 3a–d). However, it is absent (Figure 3e,f) in the Bu_4N^+ electrolyte case, indicating that this cation may be too large to be rapidly inserted into the crystal. Li^+, Na^+, and K^+ ions may be inserted into the pore made by the dissolution of K^+ and/or NC_3N^{2+} accompanying the first oxidation. The size of the pores can be estimated from the cation sizes, which give a radius of 1.65 Å[26] for K^+ and 2.8 Å × 7.0 Å for NC_3N^{2+}, both being smaller than the radius of Bu_4N^+ (4.1 Å[27]). The oxidative cyclic voltammograms for **1** in Li^+, Na^+, and K^+ electrolyte solution remained almost unchanged after a few cycles of potential. In contrast, the oxidation current with Bu_4N^+-containing electrolyte gradually decreased with each cycle, indicating loss of material.

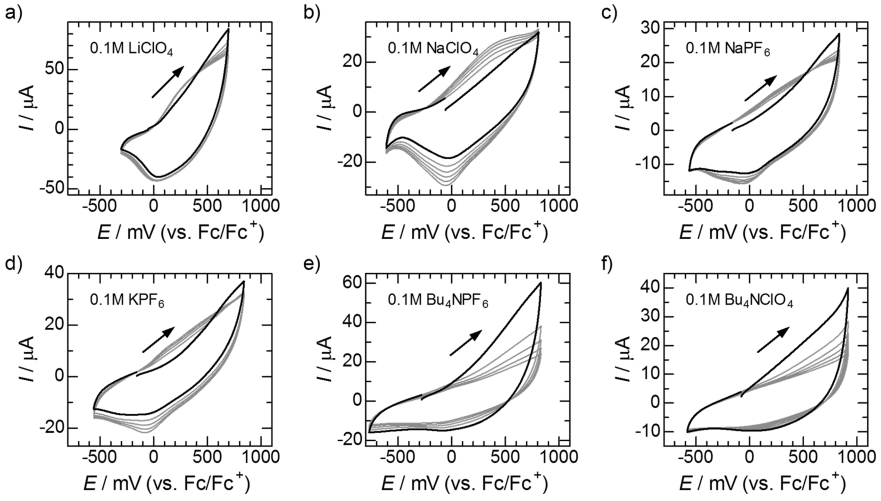

Figure 3. Cyclic voltammograms obtained at a scan rate of 100 mV s^{-1} for oxidation of a **1**-modified GC electrode in contact with (a) 0.1 M $LiClO_4$, (b) 0.1 M $NaClO_4$, (c) 0.1 M $NaPF_6$, (d) 0.1 M KPF_6, (e) 0.1 M Bu_4NPF_6, and (f) 0.1 M Bu_4NClO_4 in MeCN. First (black) and further (gray) cycles of potential.

dx.doi.org/10.1021/ic402980t | Inorg. Chem. 2014, 53, 4022−4028

In order to establish the surface change that takes place during the course of the electrochemical experiments, scanning electron microscopic (SEM) images of **1** attached to an ITO electrode were obtained before and after oxidative cyclic voltammetry (100 cycles) and oxidative bulk electrolysis for 10 min. The results are shown in Figures 4 and S5. The

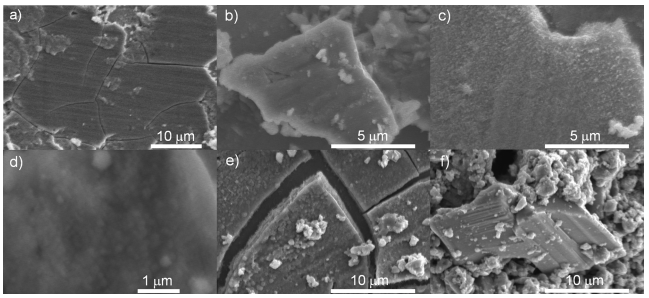

Figure 4. SEM micrograph images of **1** attached to an ITO electrode taken (a, b) prior to soaking in MeCN, (c, d) after 100 cycles of oxidative potential scan between −500 and +700 mV (vs Fc/Fc^+) at a scan rate of 100 mV s^{-1} in contact with 0.1 M $LiClO_4$ and 0.1 M $NaClO_4$ in MeCN, respectively, and (e, f) after oxidative bulk electrolysis for 10 min at +690 mV (vs Fc/Fc^+) in 0.1 M $LiClO_4$/MeCN.

characteristics of the cyclic voltammogram of **1** on the ITO electrode were almost identical to those found with the GC electrode (Figure S4). SEM images over wide regions of the surface (Figure S5a, d, g, j, and m) show that adhesion of **1** to the ITO electrode is far from homogeneous. Material is adhered to the electrode as a film with cracks (Figure 4a) or as isolated or aggregates of microcrystals (Figure 4b). After oxidative cyclic voltammetry and oxidative bulk electrolysis, an additional level of microcrystallinity was evident (Figure 4c–e), implying that oxidation and reduction components may occur via mechanisms (1) and (2).

Insertion of electrolyte cation in the companion reduction process is supported by EDX spectra obtained during collection of SEM images (Figure 5). In particular, Na is detected after oxidation of **1** in 0.1 M $NaClO_4$/MeCN but not after soaking surface-confined **1** in 0.1 M $NaClO_4$/MeCN for 30 min. This result leads to the conclusion that ingress of Na^+ into the crystal

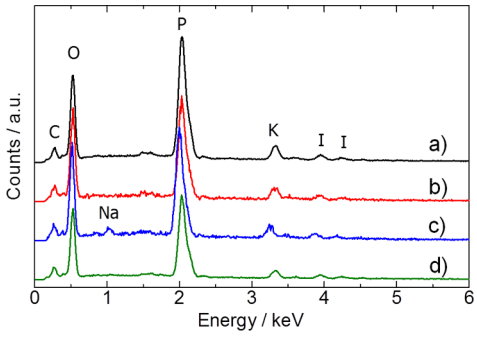

Figure 5. Energy dispersive X-ray (EDX) spectra of **1** attached to an ITO electrode measured (a) prior to soaking in MeCN (black, obtained from Figure 4a), (b, c) after 100 cycles of oxidative potential scan between −500 and +700 mV (vs Fc/Fc^+) at a scan rate of 100 mV s^{-1} in contact with 0.1 M $LiClO_4$ (red, obtained from Figure 4c) and 0.1 M $NaClO_4$ (blue, obtained from Figure 4d) in MeCN, respectively, and (d) after soaking in 0.1 M $NaClO_4$/MeCN for 30 min (green, obtained from Figure S5k).

is induced by oxidation. Cyclic voltammograms at a range of scan rates are given in Figure S6. The slope of 0.6 of a plot of $\log(i_{pc})$ versus $\log(\nu)$ (Figure S7) implies that the process is diffusion limited, and hence diffusion of Na^+ and electrons takes place through surface-confined **1**. Further details on the analysis of the scan rate dependency and the barrier to diffusion of electrons and/or Na^+ through the microcrystals are provided in the Supporting Information.

The crystal structure and lattice water molecules are believed to be maintained during the course of oxidative cycling of **1** in contact with MeCN (0.1 M $LiClO_4$ or 0.1 M $NaClO_4$) because the PXRD pattern of **1** remains almost unchanged after the 100 cycles of potentials (Figure S1d,e).

Effect of the Acid on the Oxidation of Solid 1. In order to further study the effect of H^+ in the electrolyte, $HClO_4$ (60% in water) or TFA was added to 0.1 M $LiClO_4$/MeCN or pure MeCN solutions. Figure 6a shows cyclic voltammograms in 0.1

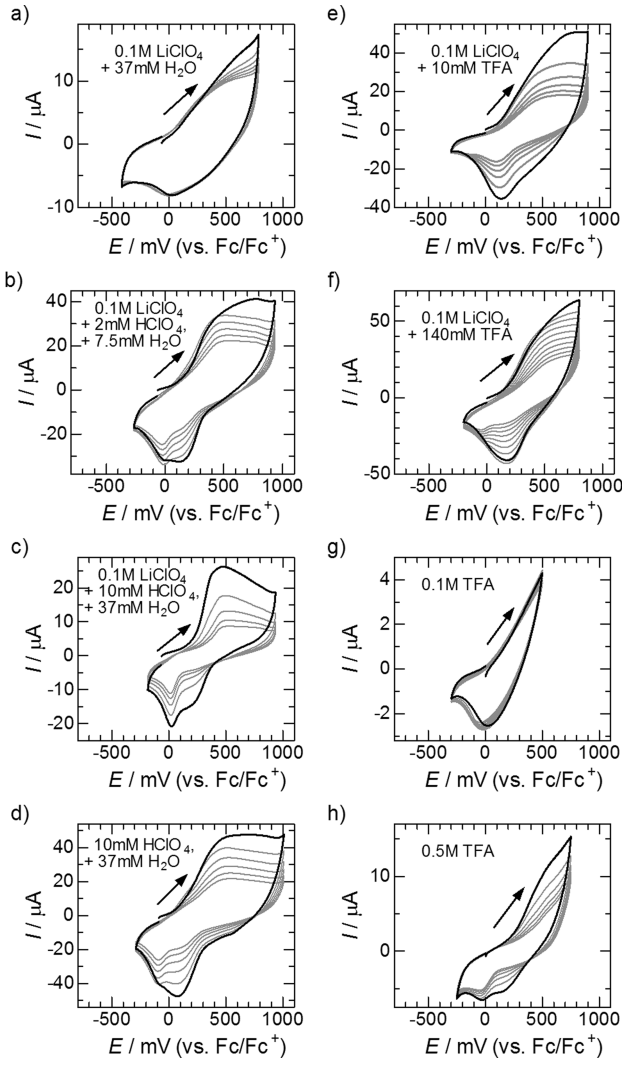

Figure 6. Cyclic voltammograms obtained at a scan rate of 100 mV s^{-1} (except for (g), at 20 mV s^{-1}) for oxidation of a **1**-modified GC electrode in contact with (a) 0.1 M $LiClO_4$, 37 mM H_2O, (b) 0.1 M $LiClO_4$, 2 mM $HClO_4$, 7.5 mM H_2O, (c) 0.1 M $LiClO_4$, 10 mM $HClO_4$, 37 mM H_2O, (d) 10 mM $HClO_4$, 37 mM H_2O, (e) 0.1 M $LiClO_4$, 10 mM TFA, (f) 0.1 M $LiClO_4$, 140 mM TFA, (g) 0.1 M TFA, and (h) 0.5 M TFA in MeCN. First (black) and further (gray) cycles of potential.

dx.doi.org/10.1021/ic402980t | Inorg. Chem. 2014, 53, 4022–4028

M $LiClO_4$/MeCN solution also containing 37 mM H_2O, which equates to the concentration of water included by addition of 10 mM aqueous $HClO_4$. Since Figures 6a and 3a are almost identical, it is concluded that the additional 37 mM H_2O does not significantly affect the voltammetry. Figure 6b and c provide examples of cyclic voltammograms in 0.1 M $LiClO_4$, 2 mM $HClO_4$, 7.5 mM H_2O/MeCN and 0.1 M $LiClO_4$, 10 mM $HClO_4$, 37 mM H_2O/MeCN, respectively. The oxidation component is now more distinct and appears at around +500 mV. This change may indicate that removal of cation (K^+ and/or NC_3N^{2+}) is facilitated by acid-enhanced dissolution of the oxidized sample. Moreover, reduction now consists of two processes, with the first (+100 to +200 mV) and the second (−100 to 0 mV) both decreasing on cycling the potential. This behavior also was found in electrolyte solution without $LiClO_4$ (Figure 6d), although in this case the voltammetry is more similar to that in Figure 6b than Figure 6c. High concentrations of Li^+ (0.1 M) and H^+ (10 mM) are necessary to obtain voltammograms like those in Figure 6c. The origin of the splitting into two reduction components might be a result of two kinds of pore provided by loss of K^+ and NC_3N^{2+} accompanying the first oxidation or more likely because reduction of bulk soluble and insoluble material occurs in the presence of acid.

In the case of addition of TFA to 0.1 M $LiClO_4$/MeCN, a decrease of current on cycling the potential is again observed, indicating dissolution of oxidized **1** (Figure 6e,f). Split reduction components were observed only on addition of a high concentration of TFA (0.14 M). TFA is a weak acid and does not completely dissociate into H^+ and CF_3COO^- in MeCN (pK_a(MeCN) = 12.7[28]). For a 0.1 M TFA solution without $LiClO_4$, oxidation of **1** (Figure 6g) was suppressed by the low concentration of dissociated electrolyte (H^+ and CF_3COO^-). In this case a higher concentration (0.5 M; Figure 6h) of TFA was necessary to observe a decrease of the oxidation current and splitting into two reduction components on cycling the potential.

As hypothesized above, oxidation of **1** induces loss of K^+ and/or NC_3N^{2+} from the solid **1** to create a pore, and electrolyte cations are then inserted in the reduction component. Although an alkali metal ion can connect the diplatinum units and hold the one-dimensional structure together via multiple coordination bonds to pop ligands, H^+ cannot fulfill this role. Therefore, under acidic conditions, it is assumed that insertion of H^+ in the reduction component reduces the extent of the coordination-bond network and enhances dissolution.

Reduction of Solid 1 in MeCN Solution Containing Different Electrolytes. In order to study the reduction of **1**, cyclic voltammograms were recorded up to approximately −860 mV (when acid is present) or −1570 mV (in the absence of acid). The results obtained in the presence of different electrolytes are shown in Figure 7. The peak potential for reduction of the microcrystal is strongly dependent on the electrolyte. In the case of solutions containing $HClO_4$, reduction occurs between −415 and −480 mV (Figure 7b,c). As the cation size increases from H^+ to Li^+ and Bu_4N^+, the reduction peak potential becomes more negative. Reduction is assumed to occur via mechanism (1) or (2). Even though reduction is irreversible, inserted cations would be required to achieve charge neutrality.

Bulk Oxidative Electrolysis of Solid 1 in 0.1 M $LiClO_4$/MeCN. Although the oxidation of **1** in 0.1 M $LiClO_4$/MeCN

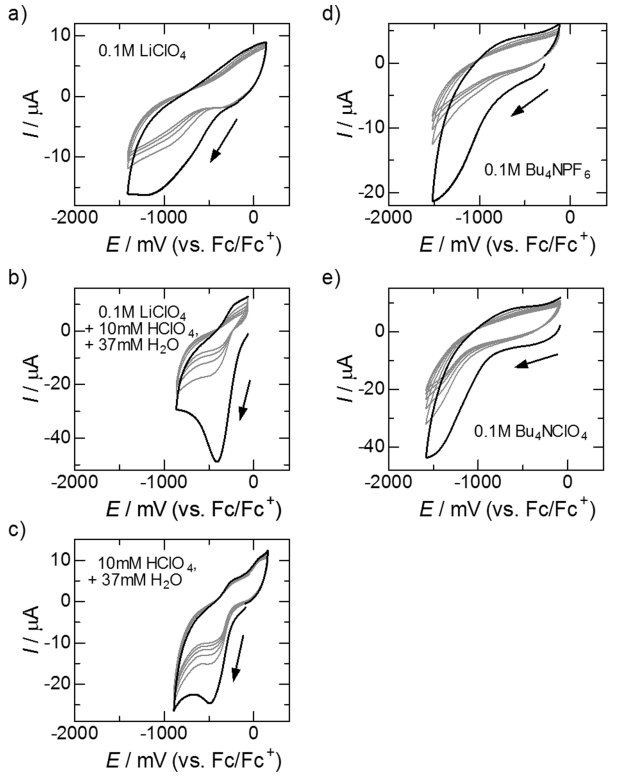

Figure 7. Cyclic voltammograms obtained at a scan rate of 100 mV s^{-1} for reduction of a **1**-modified GC electrode in contact with (a) 0.1 M $LiClO_4$, (b) 0.1 M $LiClO_4$, 10 mM $HClO_4$, 37 mM H_2O, (c) 10 mM $HClO_4$, 37 mM H_2O, (d) 0.1 M Bu_4NPF_6, and (e) 0.1 M Bu_4NClO_4 in MeCN. First (black) and further (gray) cycles of potential.

(Figure 3a) is chemically reversible, it is unclear as to whether all of the microcrystalline solid is oxidized. In order to reveal the extent of oxidation, bulk electrolysis was performed, using **1** adhered to an ITO electrode by the mechanical attachment method. The applied constant potential used for bulk electrolysis was +690 mV (vs Fc/Fc^+) and gave the charge versus time data shown in Figure 8. The amount of solid

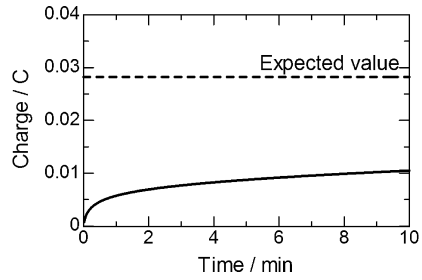

Figure 8. Charge−time data derived from bulk electrolysis at +690 mV (vs Fc/Fc^+) of a **1**-modified ITO electrode in contact with MeCN containing 0.1 M $LiClO_4$.

oxidized was calculated from Faraday's law of electrolysis: $Q = Fzm/M$, where Q is the charge, F is the Faraday constant (96485 C mol^{-1}), z is the number of electrons transferred per electroactive species (one assumed in this case), m is the mass of **1** attached to the GC electrode (0.386 mg), and M is the molar mass of **1** (1319.3 g mol^{-1}). After about 5 min of bulk electrolysis, the charge reached a limiting value of about 0.01 C, which represents about 30% of the sample being oxidized.

dx.doi.org/10.1021/ic402980t | Inorg. Chem. 2014, 53, 4022−4028

Incomplete electrolysis can be explained by noting that solid **1** is a semiconductor in its initial state with platinum being in a Pt^{2+}/Pt^{3+} mixed-valence state. However, when the 1D chain is oxidized to the Pt^{3+} state, the compound becomes an insulator, which limits the extent of oxidation. In fact, some microcrystals of the surface-confined **1** solid are not modified by bulk electrolysis (Figure 4f) contrary to the film of **1** (Figure 4e). This result is opposite that for electrochemical solid−solid-state formation of conductive metal−TCNQ complexes from an insulating TCNQ solid adhered to an electrode in contact with an aqueous metal salt solution.[29] The lowering of conductivity may be minimized in a single crystal, because the doped hole can move along the larger domain.

CONCLUSION

The voltammetry of surface-attached semiconducting solid **1** has been achieved with a chemically modified electrode in contact with MeCN-containing electrolyte. The oxidation of **1** was almost chemically reversible when either Li^+, Na^+, or K^+ was present in the electrolyte, whereas the coupled reduction component was not observed with a Bu_4N^+-containing electrolyte solution presumably because this cation is too large to be inserted into the crystal. The presence of H^+ enhanced dissolution of the oxidized sample and led to splitting in the coupled reduction process, plausibly originating from two different pores made by the egress of K^+ (1.65 Å[26] in radius) and NC_3N^{2+} (2.8 Å × 7.0 Å) upon oxidation. The reduction of **1** was also affected by the electrolyte cation size. As the size increased from H^+ to Bu_4N^+, the potential for reduction becomes less negative. The oxidation of **1** did not progress completely because the mixed-valence domains disappear as **1** is oxidized. However, the ability to achieve reversible chemical oxidation of **1** suggests that this material could be used as the positive electrode material in a rechargeable battery. By combining solid-state optical and electrochemical data, the energies of the valence and conduction bands of **1** are estimated to be approximately −5.38 and −4.53 eV, respectively (see Supporting Information). Thus, the energy difference between the valence band and the reversible Li/Li^+ potential is about 4 V, which is comparable to the cell voltage of a conventional Li-ion rechargeable battery. These results should open new avenues of research related to the electrochemical dissolution/insertion behavior in MMX chains and other conductive solid coordination compounds. The electrochemical doping of dehydrated **1**, which has a larger pore than the presently studied hydrated complex, provides the next challenge to achieve an electrochemically active porous coordination compound. The structure of dehydrated **1** is maintained even after immersion in MeCN (Figure S2).

ASSOCIATED CONTENT

Supporting Information

Figures S1 to S7, Table S1, experimental details, and estimation of the band energies are available free of charge via the Internet at http://pubs.acs.org.

AUTHOR INFORMATION

Corresponding Authors

*E-mail: h-iguchi@m.tohoku.ac.jp.
*E-mail: alan.bond@monash.edu.

Author Contributions

The manuscript was written on the basis of significant contributions from all authors, who have given their approval for publication of the manuscript.

Notes

The authors declare no competing financial interest.

ACKNOWLEDGMENTS

We acknowledge Dr. Kajimoto, Mr. Hanagata, and Prof. Nishizawa at Tohoku University for acquiring the SEM images and EDX spectra. This work was financially supported by a Grant-in-Aid for Scientific Research (S) (Grant No. 20225003) from the Ministry of Education, Culture, Sports, Science, and Technology, Japan (M.Y.), by a JSPS Research Fellowships for Young Scientists (H.I.), by the Tohoku University Institute for International Advanced Research and Education (H.I.), by the Sumitomo Foundation (H.I.), and the Australian Research Council (A.B.). A.N. would like to thank Scientific Research at King Saud University for funding through the Research Group Project No. RGP-VPP-236.

REFERENCES

(1) Suh, M. P.; Park, H. J.; Prasad, T. K.; Lim, D.-W. *Chem. Rev.* **2012**, *112*, 782−835.
(2) (a) Sumida, K.; Rogow, D. L.; Mason, J. A.; McDonald, T. M.; Bloch, E. D.; Herm, Z. R.; Bae, T.-H.; Long, J. R. *Chem. Rev.* **2012**, *112*, 724−781. (b) Li, J.-R.; Sculley, J.; Zhou, H.-C. *Chem. Rev.* **2012**, *112*, 869−932.
(3) (a) Lee, J.; Farha, O. K.; Roberts, J.; Scheidt, K. A.; Nguyen, S. T.; Hupp, J. T. *Chem. Soc. Rev.* **2009**, *38*, 1450−1459. (b) Yoon, M.; Srirambalaji, R.; Kim, K. *Chem. Rev.* **2012**, *112*, 1196−1231.
(4) (a) Kurmoo, M. *Chem. Soc. Rev.* **2009**, *38*, 1353−1379. (b) Coronado, E.; Espallargas, G. M. *Chem. Soc. Rev.* **2013**, *42*, 1525−1539.
(5) (a) Furukawa, Y.; Ishikawa, T.; Sugikawa, K.; Kokado, K.; Sada, K. *Angew. Chem., Int. Ed.* **2012**, *51*, 10566−10569. (b) Ishikawa, T.; Furukawa, Y.; Sugikawa, K.; Kokado, K.; Sada, K. *J. Am. Chem. Soc.* **2013**, *135*, 5427−5432.
(6) Inokuma, Y.; Yoshioka, S.; Ariyoshi, J.; Arai, T.; Hitora, Y.; Takada, K.; Matsunaga, S.; Rissanen, K.; Fujita, M. *Nature* **2013**, *495*, 461−466.
(7) Morozan, A.; Jaouen, F. *Energy Environ. Sci.* **2012**, *5*, 9269−9290.
(8) (a) Férey, G.; Millange, F.; Morcrette, M.; Serre, C.; Doublet, M.-L.; Greneche, J.-M.; Tarascon, J.-M. *Angew. Chem., Int. Ed.* **2007**, *46*, 3259−3263. (b) Demir-Cakan, R.; Morcrette, M.; Nouar, F.; Davoisne, C.; Devic, T.; Gonbeau, D.; Dominko, R.; Serre, C.; Férey, G.; Tarascon, J.-M. *J. Am. Chem. Soc.* **2011**, *133*, 16154−16160.
(9) Lee, D. Y.; Yoon, S. J.; Shrestha, N. K.; Lee, S.-H.; Ahn, H.; Han, S.-H. *Microporous Mesoporous Mater.* **2012**, *153*, 163−165.
(10) (a) Nagao, Y.; Fujishima, M.; Ikeda, R.; Kanda, S.; Kitagawa, H. *Synth. Met.* **2003**, *133*, 431−432. (b) Hurd, J. A.; Vaidhyanathan, R.; Thangadurai, V.; Ratcliffe, C. I.; Moudrakovski, I. L.; Shimizu, G. K. H. *Nat. Chem.* **2009**, *1*, 705−710. (c) Bureekaew, S.; Horike, S.; Higuchi, M.; Mizuno, M.; Kawamura, T.; Tanaka, D.; Yanai, N.; Kitagawa, S. *Nat. Mater.* **2009**, *8*, 831−836. (d) Dey, C.; Kundu, T.; Banerjee, R. *Chem. Commun.* **2012**, *48*, 266−268. (e) Sadakiyo, M.; Okawa, H.; Shigematsu, A.; Ohba, M.; Yamada, T.; Kitagawa, H. *J. Am. Chem. Soc.* **2012**, *134*, 5472−5475. (f) Xu, G.; Otsubo, K.; Yamada, T.; Sakaida, S.; Kitagawa, H. *J. Am. Chem. Soc.* **2013**, *135*, 7438−7441.
(11) Lee, D. Y.; Shinde, D. V.; Yoon, S. J.; Cho, K. N.; Lee, W.; Shrestha, N. K.; Han S.-H. *J. Phys. Chem. C* [online early access]. DOI: 10.1021/jp4079663. Published online: Nov 1, 2013. http://pubs.acs.org/doi/abs/10.1021/jp4079663 (accessed Nov 1, 2013).
(12) Wade, C. R.; Li, M.; Dincă, M. *Angew. Chem., Int. Ed.* **2013**, *52*, 13377−13381.

(13) (a) Wires, B. M..; Foo, M.-L.; Balsara, N. P.; Long, J. R. *J. Am. Chem. Soc.* **2011**, *133*, 14522−14525. (b) Ameloot, R.; Aubrey, M.; Wires, B. M..; Gómora-Figueroa, A. P.; Patel, S. N.; Balsara, N. P.; Long, J. R. *Chem.—Eur. J.* **2013**, *19*, 5533−5536. (c) Aubrey, M. L.; Ameloot, R.; Wires, B. M.; Long, J. R. *Energy Environ. Sci.* **2014**, *7*, 667−671.
(14) Fuma, Y.; Ebihara, M.; Kutsumizu, S.; Kawamura, T. *J. Am. Chem. Soc.* **2004**, *126*, 12238−12239.
(15) (a) Takaishi, S.; Hosoda, M.; Kajiwara, T.; Miyasaka, H.; Yamashita, M.; Nakanishi, Y.; Kitagawa, Y.; Yamaguchi, K.; Kobayashi, A.; Kitagawa, H. *Inorg. Chem.* **2009**, *48*, 9048−9050. (b) Kobayashi, Y.; Jacobs, B.; Allendorf, M. D.; Long, J. R. *Chem. Mater.* **2010**, *22*, 4120−4122.
(16) (a) Nguyen, T. L. A.; Demir-Cakan, R.; Devic, T.; Morcrette, M.; Ahnfeldt, T.; Auban-Senzier, P.; Stock, N.; Goncalves, A.-M.; Filinchuk, Y.; Tarascon, J.-M.; Férey, G. *Inorg. Chem.* **2010**, *49*, 7135−7143. (b) Narayan, T. C.; Miyakai, T.; Seki, S.; Dincă, M. *J. Am. Chem. Soc.* **2012**, *134*, 12932−12935.
(17) (a) Robin, M. B.; Day, P. *Adv. Inorg. Chem. Radiochem.* **1968**, *10*, 247−422. (b) Day, P. In *Low-Dimensional Cooperative Phenomena*; Keller, H. J., Ed.; Plenum Press: New York, 1974; pp 191−214.
(18) (a) Kuwabara, M.; Yonemitsu, K. *J. Phys. Chem. Solids* **2001**, *62*, 435−438. (b) Kuwabara, M.; Yonemitsu, K. *J. Mater. Chem.* **2001**, *11*, 2163−2175.
(19) (a) Bellitto, C.; Flamini, A.; Gastaldi, L.; Scaramuzza, L. *Inorg. Chem.* **1983**, *22*, 444−449. (b) Bellitto, C.; Dessy, G.; Fares, V. *Inorg. Chem.* **1985**, *24*, 2815−2820. (c) Clark, R. J. H.; Walton, J. R. *Inorg. Chim. Acta* **1987**, *129*, 163−171. (d) Kitagawa, H.; Onodera, N.; Sonoyama, T.; Yamamoto, M.; Fukawa, T.; Mitani, T.; Seto, M.; Maeda, Y. *J. Am. Chem. Soc.* **1999**, *121*, 10068−10080. (e) Mitsumi, M.; Murase, T.; Kishida, H.; Yoshinari, T.; Ozawa, Y.; Toriumi, K.; Sonoyama, T.; Kitagawa, H.; Mitani, T. *J. Am. Chem. Soc.* **2001**, *123*, 11179−11192. (f) Mitsumi, M.; Kitamura, K.; Morinaga, A.; Ozawa, Y.; Kobayashi, M.; Toriumi, K.; Iso, Y.; Kitagawa, H.; Mitani, T. *Angew. Chem., Int. Ed.* **2002**, *41*, 2767−2771. (g) Otsubo, K.; Kobayashi, A.; Kitagawa, H.; Hedo, M.; Uwatoko, Y.; Sagayama, H.; Wakabayashi, Y.; Sawa, H. *J. Am. Chem. Soc.* **2006**, *128*, 8140−8141. (h) Mitsumi, M.; Yoshida, Y.; Kohyama, A.; Kitagawa, Y.; Ozawa, Y.; Kobayashi, M.; Toriumi, K.; Tadokoro, M.; Ikeda, N.; Okumura, M.; Kurmoo, M. *Inorg. Chem.* **2009**, *48*, 6680−6691. (i) Kobayashi, A.; Kitao, S.; Seto, M.; Ikeda, R.; Kitagawa, H. *Inorg. Chem.* **2009**, *48*, 8044−8049. (j) Otsubo, K.; Kobayashi, A.; Hedo, M.; Uwatoko, Y.; Kitagawa, H. *Chem. Asian J.* **2009**, *4*, 1673−1676. (k) Welte, L.; Garcia-Couceiro, U.; Castillo, O.; Olea, D.; Polop, C.; Guijarro, A.; Luque, A.; Gomez-Rodriguez, J. M.; Gomez-Herrero, J.; Zamora, F. *Adv. Mater.* **2009**, *21*, 2025−2028. (l) Ikeuchi, S.; Yamamura, Y.; Yoshida, Y.; Mitsumi, M.; Toriumi, K.; Saito, K. *Bull. Chem. Soc. Jpn.* **2010**, *83*, 261−266. (m) Welte, L.; Calzolari, A.; Felice, R. D.; Zamora, F.; Gomez-Herrero, J. *Nat. Nanotechnol.* **2010**, *5*, 110−115. (n) Guijarro, A.; Castillo, O.; Welte, L.; Calzolari, A.; Miguel, P. J. S.; Gomez-Garcia, C. J.; Olea, D.; Felice, R. D.; Gomez-Herrero, J.; Zamora, F. *Adv. Funct. Mater.* **2010**, *20*, 1451−1457. (o) Mas-Balleste, R.; Gomez-Herrero, J.; Zamora, F. *Chem. Soc. Rev.* **2010**, *39*, 4220−4233. (p) Mitsumi, M.; Yamashita, T.; Aiga, Y.; Toriumi, K.; Kitagawa, H.; Mitani, T.; Kurmoo, M. *Inorg. Chem.* **2011**, *50*, 4368−4377.
(20) (a) Che, C.-M.; Herbstein, F. H.; Schaefer, W. P.; Marsh, R. E.; Gray, H. B. *J. Am. Chem. Soc.* **1983**, *105*, 4604−4607. (b) Kurmoo, M.; Clark, R. J. H. *Inorg. Chem.* **1985**, *24*, 4420−4425. (c) Clark, R. J. H.; Kurmoo, M.; Dawes, H. M.; Hursthouse, M. B. *Inorg. Chem.* **1986**, *25*, 409−412. (d) Butler, L. G.; Zietlow, M. H.; Che, C.-M.; Schaefer, W. P.; Sridhar, S.; Grunthaner, P. J.; Swanson, B. I.; Clark, R. J. H.; Gray, H. B. *J. Am. Chem. Soc.* **1988**, *110*, 1155−1162. (e) Stroud, M. A.; Drickamer, H. G.; Zietlow, M. H.; Gray, H. B.; Swanson, B. I. *J. Am. Chem. Soc.* **1989**, *111*, 66−72. (f) Mitani, T.; Wada, Y.; Yamashita, M.; Toriumi, K.; Kobayashi, A.; Kobayashi, H. *Synth. Met.* **1994**, *64*, 291−294. (g) Yamashita, M.; Miya, S.; Kawashima, T.; Manabe, T.; Sonoyama, T.; Kitagawa, H.; Mitani, T.; Okamoto, H.; Ikeda, R. *J. Am. Chem. Soc.* **1999**, *121*, 2321−2322. (h) Matsuzaki, H.; Matsuoka, T.; Kishida, H.; Takizawa, K.; Miyasaka, H.; Sugiura, K.; Yamashita, M.; Okamoto, H. *Phys. Rev. Lett.* **2003**, *90*, 046401−1−4. (i) Mastuzaki, H.; Kishida, H.; Okamoto, H.; Takizawa, K.; Matsunaga, S.; Takaishi, S.; Miyasaka, H.; Sugiura, K.; Yamashita, M. *Angew. Chem., Int. Ed.* **2005**, *44*, 3240−3243. (j) Yamashita, M.; Takaishi, S.; Kobayashi, A.; Kitagawa, H.; Matsuzaki, H.; Okamoto, H. *Coord. Chem. Rev.* **2006**, *250*, 2335−2346. (k) Yamashita, M.; Takizawa, K.; Matsunaga, S.; Kawakami, D.; Iguchi, H.; Takaishi, S.; Kajiwara, T.; Iwahori, F.; Ishii, T.; Miyasaka, H.; Sugiura, K.; Matsuzaki, H.; Kishida, H.; Okamoto, H. *Bull. Chem. Soc. Jpn.* **2006**, *79*, 1404−1406. (l) Iguchi, H.; Takaishi, S.; Kajiwara, T.; Miyasaka, H.; Yamashita, M.; Matsuzaki, H.; Okamoto, H. *J. Inorg. Organomet. Polym. Mater.* **2009**, *19*, 85−90. (m) Iguchi, H.; Jiang, D.; Xie, J.; Takaishi, S.; Yamashita, M. *Polymers* **2011**, *3*, 1652−1661.
(21) (a) Iguchi, H.; Takaishi, S.; Kajiwara, T.; Miyasaka, H.; Yamashita, M.; Matsuzaki, H.; Okamoto, H. *J. Am. Chem. Soc.* **2008**, *130*, 17668−17669. (b) Iguchi, H.; Takaishi, S.; Miyasaka, H.; Yamashita, M.; Matsuzaki, H.; Okamoto, H.; Tanaka, H.; Kuroda, S. *Angew. Chem., Int. Ed.* **2010**, *49*, 552−555. (c) Iguchi, H.; Takaishi, S.; Breedlove, B. K.; Yamashita, M.; Matsuzaki, H.; Okamoto, H. *Inorg. Chem.* **2012**, *51*, 9967−9977.
(22) Iguchi, H.; Takaishi, S.; Jiang, D.; Xie, J.; Yamashita, M.; Uchida, A.; Kawaji, H. *Inorg. Chem.* **2013**, *52*, 13812−13814.
(23) (a) Bryan, S. A.; Dickson, M. K.; Roundhill, D. M. *J. Am. Chem. Soc.* **1984**, *106*, 1882−1883. (b) Bryan, S. A.; Schmehl, R. H.; Roundhill, D. M. *J. Am. Chem. Soc.* **1986**, *108*, 5408−5412. (c) Bennett, M. A.; Bhargava, S. K.; Bond, A. M.; Bansal, V.; Forsyth, C. M.; Guo, S.-X.; Privér, S. H. *Inorg. Chem.* **2009**, *48*, 2593−2604.
(24) (a) Bond, A. M.; Cooper, J. B.; Marken, F.; Way, D. M. *J. Electroanal. Chem.* **1995**, *396*, 408−418. (b) Bond, A. M. *Broadening Electrochemical Horizons*; Oxford University Press: Oxford, 2002; Chapter 5. (c) Scholz, F.; Schröder, U.; Gulabowski, R. *Electrochemistry of Immobilised Particles and Droplets*; Springer: Berlin, 2005.
(25) Murphy, D. W.; Rosseinsky, M. J. *Chemical Physics of Intercalation II*; Bernier, P.; Fischer, J. E.; Roth, S.; Solin, S. A., Eds.; Plenum: New York, 1993.
(26) Shannon, R. D. *Acta Crystallogr.* **1976**, *A32*, 751−767.
(27) Marcus, Y. *Biophys Chem.* **1994**, *51*, 111−127.
(28) Izutsu, K. *Acid−Base Dissociation Constants in Dipolar Aprotic Solvents: International Union of Pure and Applied Chemistry Chemical Data Series No. 35*; Blackwell Scientific: Oxford, 1990; pp 17−35.
(29) (a) Nafady, A.; O'Mullane, A. P.; Bond, A. M.; Neufeld, A. K. *Chem. Mater.* **2006**, *18*, 4375−4384. (b) O'Mullane, A. P.; Fay, N.; Nafady, A.; Bond, A. M. *J. Am. Chem. Soc.* **2007**, *129*, 2066−2073. (c) Nafady, A.; Bond, A. M.; Bilyk, A.; Harris, A. R.; Bhatt, A. I.; O'Mullane, A. P.; Marco, R. D. *J. Am. Chem. Soc.* **2007**, *129*, 2369−2382. (d) Nafady, A.; Bond, A. M.; O'Mullane, A. P. *Inorg. Chem.* **2009**, *48*, 9258−9270. (e) Le, T. H.; Nafady, A.; Lu, J.; Peleckis, G.; Bond, A. M.; Martin, L. L. *Eur. J. Inorg. Chem.* **2012**, 2889−2897. (f) Nafady, A.; Bond, A. M.; Qu, V.; Martin, L. L. *J. Solid State Electrochem.* **2013**, *17*, 1609−1620.